Victoria-Hernandez, J.; Yi, S.; Bohlen, J.; Kurz, G.; Letzig, D.:

The influence of the recrystallization mechanisms and grain growth on the texture of a hot rolled AZ31 sheet during subsequent isochronal annealing

In: Journal of Alloys and Compounds (2014) Elsevier

DOI: 10.1016/j.jallcom.2014.07.083

The influence of the recrystallization mechanisms and grain growth on the texture of a hot rolled AZ31 sheet during subsequent isochronal annealing

J. Victoria-Hernandez, S. Yi, J. Bohlen, G. Kurz, D. Letzig

Magnesium Innovation Centre MagIC, Helmholtz-Zentrum Geesthacht, Max-Planck-Strasse 1, D-21502 Geesthacht, Germany

Abstract

The texture development during isochronal annealing at 250, 300 and 350 °C for 30 min of a hot rolled Mg AZ31 sheet produced by twin-roll casting was studied in this work. It was found that the rolling texture shows some features that resemble the textures that develop in rolled Mg alloys with rare earth additions. During further heat treatment, special attention was given to the deformation and recrystallization mechanisms, and grain growth that control the texture development. It was found that at 250 and 300 °C extended recovery and discontinuous recrystallization influence the texture by generating strain free grains with off-basal orientation. Conversely, during annealing at 350 °C growth of grains with their c-axis close to the (0001) leads to the formation of the well-known basal type texture.

Keywords: Recovery, Deformation mechanisms, Recrystallization mechanisms, Texture

1. Introduction

Typical magnesium sheets like those of the AZ- or ZM-alloy series develop strong textures during rolling with a preferred orientation of basal planes parallel to the sheet plane. This sheet texture is also known as “basal type” texture. Such a texture limits the ability of basal slip to accommodate plastic strain in the sheet plane and is thus unfavourable for the work hardening ability of the sheet, its ductility and formability, especially at room temperature. Recently, the use of rare earths (RE) as alloying elements has attracted attention since they can influence the texture development during sheet rolling. It has also been discussed that RE-addition lead to changes in the recrystallization and grain growth behaviour of wrought alloy sheets during subsequent heat treatments [1]. As a result, weak textures develop and a substantial increase in their ductility and formability has been observed [2].

These weaker textures no longer exhibit a distinct basal fibre component, but tend to show off-basal peaks and a broader orientation distribution of the basal planes towards the transverse direction (TD) rather than towards the rolling direction (RD) [3, 4]. Nevertheless,

the governing mechanisms for the formation of the distinct textures of Mg-RE alloys are still under discussion. In the context of Mg alloys with additions of RE elements, there is evidence that deformation mechanisms change their balance during rolling e.g. the activation of non-basal slip increases or a more pronounced activation of contraction twinning or double twinning can lead to nucleation of grains with different orientations [1]. Yet, so far the plausible explanation of the origin of the texture modification in RE-containing Mg alloys has been associated with changes that occur mainly during the recrystallization process [5]. For instance, it has been discussed that particle stimulated nucleation (PSN) of recrystallization as a recrystallization mechanism can influence the texture development during deformation [6, 7], as well as a nucleation and growth of grains within shear bands that also contribute to texture modification [8]. However, the former mechanism has a little influence in the texture development due to the low fraction of the microstructure that can be formed. Recently, restricted grain growth mechanisms in RE added alloys have received attention in regard to solute segregations or particle pinning which could be one reason for the development of weak and distinct textures in Mg-RE alloys [9]. However, the effect of particle pinning is not limited to RE containing alloys, it has been pointed out that is possible to retain non-basal orientations in a conventional AZ31 alloy due to precipitation of $Mg_{17}Al_{12}$ on grain boundaries that restrict grain growth [10, 11]. This finding suggests that some mechanisms that influence the texture development to the ones present in RE-added Mg alloys could be found in RE-free Mg alloys.

Accordingly, in this study we have performed hot rolling experiments using the “conventional” AZ31 alloy produced by twin-roll casting in an attempt to balance the growth of potential texture changing fractions of grains which are a result of different deformation and recrystallization mechanisms followed by grain growth. It was noted that after hot rolling the rolling texture of the twin roll cast AZ31 exhibited features that resemble the texture that develops in Mg alloys with RE additions. Consequently, isochronal heat treatments performed at 250, 300 and 350 °C were carried out in order to reveal the mechanisms (i.e. recovery, continuous and discontinuous static recrystallization and growth of grains) involved in the microstructural development and relate them with changes in the final recrystallization texture. The temperatures used in this work were selected to slow down the recrystallization kinetics during the heat treatment in an attempt to reveal the recrystallization mechanism involved during microstructure development. This allows us to retain features of the microstructure (especially at the lowest temperature) which were related them with a respective mechanism.

This RE free alloy is used bearing in mind that the formation of the basal type would be a result of a higher significance of one of those mechanisms.

2. Experimental procedure

Twin roll cast (TRC) AZ31 strip with an initial thickness of 5.7 mm was rolled to a final thickness of 1.9 mm at 450 °C. The rolling procedure used in this work consisted in four rolling passes with a degree of deformation for the first pass of φ=0.1 (true strain), followed by three passes with φ=0.3. In order to avoid edge cracking, the rollers were also heated up to 230 °C. Before the first pass and after the following rolling passes, the rolled samples were reheated to the rolling temperature for 20 min. After the final rolling pass the sheet was air cooled.

Samples were cut after the final rolling pass and the microstructures were analysed in as-rolled condition (AR) and annealed at 250, 300 and 350 °C for 30 min using optical microscopy and electron backscatter diffraction (EBSD) in a field emission gun scanning electron microscope (Zeiss^{TM}, Ultra 55) equipped with an EDAX/TSL EBSD system.

Samples were prepared on the RD-normal direction (ND) plane. They were mechanically ground with SiC paper (grit 800-2500) and polished with oxide polishing suspension of 0.05 μm. The polished samples were chemically etched with a picric acid solution (150 ml of ethanol, 40 ml distilled water, 6.5 ml acetic acid and 3-4 g picric acid). The average grain size of the optical microstructures was calculated using the linear intercept method.

In the case of the EBSD samples, after the grinding process, electrochemical polishing was carried out using a Struers^{TM} AC2 solution at 16 V for 70 s at -25 °C. EBSD measurements were performed in the mid plane of the sheets using an accelerating voltage of 15 kV and a step size of 0.3 μm.

EBSD analysis was performed using inverse pole figure maps (IPF), image quality maps (IQ), grain orientation spread (GOS) and Kernel average misorientation (KAM) with the TSL OIM Analysis 6.1 software. For the EBSD analysis, only grains with confidence index higher than 0.05 were taken into account.

An analysis of the microstructure development was carried out using ex-situ EBSD measurements on a sample heat treated at 250 °C for 3 and 15 min. To do this, a sample was prepared using the method mentioned above and measured using the same EBSD settings. Once the sample was measured in as-rolled condition, it was subjected to an intermediate heat treatment in a conventional furnace filled with Argon to avoid corrosion of the sample. Before

reinserting the sample in the microscope chamber, the heat treated sample was washed with a solution of 100 ml ethanol and 0.5 ml of nitric acid to remove any layer of oxide.
Quantitative texture measurements as-cast, as-rolled and heat treated samples were carried out with a Panalytical™ X-ray diffractometer in reflection geometry using Cu-Kα radiation. Six pole figures, (0001), $(10\bar{1}0)$, $(10\bar{1}1)$, $(10\bar{1}2)$, $(10\bar{1}3)$ and $(11\bar{2}0)$, were measured up to a tilt angle of 70°. The data were used to calculate the complete orientation distribution function. The orientation distribution function was calculated using the MTEX toolbox [12] and the results are presented in terms of the (0001) and $(10\bar{1}0)$ pole figures.

3. Results and discussion

The microstructure of the twin roll cast strip is presented in Fig. 1a. The microstructure shows columnar grains growing from the surface to the centre of the strip. In the mid-section, the microstructure exhibits finer grains than in the outer zones. The strip also shows a weak texture with an alignment of the basal planes parallel to the rolling plane (Fig. 1c). More details about the twin roll casting procedure can be found in [13].
The microstructure of the hot rolled sheet is presented in Fig. 1b. The microstructure is composed by of a combination of small equiaxed grains and deformed elongated grains. The small grains are located along shear bands that develop during rolling passes. This sample has a strong deformation texture. As depicted in Fig. 1d, the texture shows a double peak with a split of 10-15 ° to RD and a markedly angular distribution towards the transverse direction (TD). In order to reveal further details of the microstructure in this condition the microstructure was characterized using EBSD. In Fig. 2a the IPF map shows that most grains present in the deformed microstructure have orientations with basal planes aligned close to the (0001) orientation. However, there are large elongated grains (coloured in green) having an off-basal orientation, i.e. a c-axis tilt towards TD. As a distinct characteristic, the elongated grains with orientations close to $(2\bar{1}\bar{1}0)$ do not contain a large amount of twins whereas others with orientations close to (0001) do. In order to analyse the orientations of the elongated grains as well as twins, their area fractions are separately presented in Fig. 2b. The large elongated grains reveal both, on one hand an orientation tilted to the RD (grain 1) and on the other hand orientations with tilt to the TD (grain 2). The former orientations can be indicative for a distinctive activity of ⟨c+a⟩ slip operative during the deformation of this type of grain as e.g. reported by Agnew et al. [14]. Conversely, the latter orientations have been recognized in the context of enhanced activation of prismatic ⟨a⟩ slip which can contribute to a texture with

broader angular distribution of basal planes towards TD [15-17]. It is known that the activation of non-basal slip such as prismatic ⟨a⟩ slip and pyramidal ⟨c+a⟩ slip is eased due to a reduction on the critical resolved shear stress (CRSS) with increasing temperature [18]. Therefore it is not surprising that at the present rolling temperature either prismatic or pyramidal slip were the dominant deformation mechanisms active for the formation of such elongated grains. It is worth mentioning that is very likely that these elongated grains are related with parts of the as-cast microstructure that underwent deformation but not recrystallization. Besides, the formation of long elongated grains seems to be typical of others hexagonal close packed materials such as Zr and Ti [19, 20]. Wagner et al. [20] observed the formation of elongated grains along the RD during cold rolling of T40 titanium sheets that were "resistant" to recrystallization during subsequent annealing. Their TEM investigations show that such grains do not contain a significant amount of twins or deformation bands. The nature of this specific type of grains in Mg alloys [15] and in Ti alloys [20] has been explained by prismatic ⟨a⟩ slip that determines deformation during the rolling passes.

It is visible in Fig. 2a that the appearance of elongated grains in the microstructure and their related orientations leads to distinctive changes in the rolling texture as show in Fig. 2b.

In addition to elongated grains with off-basal orientation, it is also recognized in Fig. 2b, that twining occurs principally in the long grains having orientation close to (0001). Those were identified mainly as a $\{10\bar{1}1\}$-$\{10\bar{1}2\}$ double twins which can also promote the splitting along RD [21]. It is noteworthy that these twins also contribute to the off-basal character of the texture of the sheet as seen in Fig. 2b (marked as orientation 3). Still, a low contribution to the bulk texture is expected due to the very small area fraction covered by such twins.

As well as the specific considerations about the deformation mechanisms addressed above, a more general approach to distinguish deformed and recrystallized fractions of the microstructure was carried out. There are two main approaches to extract the recrystallized fraction of the microstructure from EBSD data [22]. The first is to analyse the IQ maps. In this type of analysis the sharpness of the diffraction patterns is directly related with the content of defects of the surface diffracting region. The second approach relates the recrystallized fraction of the microstructure with very small variations of the crystal orientation within a region i.e. a misorientation based approach. Fig. 2c and 2d present the deformed and recrystallized fractions of the microstructure using the assumption that recrystallized grains should have a rather low internal grain-interior orientation spread (GOS) i.e. misorientation base approach [10, 19, 23]. A validation of the present misorientation approach will be shown in Fig. 6. Subsequently, grains having GOS > 0.5 ° are considered as

a part of the deformed microstructure (Fig. 2c) while any grain with GOS < 0.5 ° is accounted for the recrystallized fraction (Fig. 2d). The value of 0.5° is arbitrarily chosen in order to separate fractions of the microstructure with low inner grain misorientation.

The deformed fraction of the microstructure shows a stronger texture intensity than the counterpart recrystallized fraction, and it is characterized by the broad angular distribution of the basal planes towards TD and a component $<10\bar{1}0>$ //RD. In contrast, the recrystallized grains exhibit a weak texture and the basal type texture develops even though they were partly originated in zones with high deformation e.g. shear bands. However, based on the nature of the sheet, being hot rolled and subsequently air-cooled, it is not possible at this point to distinguish if those grains underwent DRX during the final rolling pass and/or static recrystallization (SRX) during the cooling procedure.

In order to track the microstructure development and related texture changes during further SRX, isochronal annealing for 30 min at different temperatures was carried out. Fig. 3a shows the optical microstructure and its related global texture for a sample annealed at 250 °C. It can be observed that the deformed microstructure has been replaced by a homogeneous microstructure with small grains. The average grain size is 6.4±3.1 µm. At this temperature, texture weakening is observed and the texture after heat treatment keeps some of the features from the deformation texture i.e. the broad spread to TD and the component $<10\bar{1}0>$ //RD. The same holds for the sample annealed at 300 °C and the grain size is rather similar of 7.0±4.3 µm (Fig. 3b). The microstructure of the sample treated at 350 °C exhibits a comparable microstructure and a similar grain size of 7.6±3.5 µm, but there is a noticeable sharpening of the texture intensity and their angular distribution of the basal planes towards TD is reduced. Another aspect to recall is that no secondary phase particles of $Mg_{17}Al_{12}$ were observed. This means that the particle pinning can be discarded as the responsible for the retention of the broad distribution of basal planes towards TD.

Details from the microstructures after heat treatments are revealed using IPF maps in Fig. 4. It can be observed especially in the samples heat treated at 250 and 300 °C that there are relatively large grains with orientations close to $(2\bar{1}\bar{1}0)$. In several of those grains there is the formation and coalescence of low angle grain boundaries (LAGB) (see the arrows and the inset in Fig. 4a and Fig. 4b). The presence of grains with evidence of internal substructures of LAGB is significantly reduced in the sample treated at 350 °C (Fig. 4c). The micro-textures calculated from the IPF maps are in good agreement with the global textures presented in Fig. 3. It is important to highlight that there is evidence of the formation of new grains in which most likely extended recovery was an active mechanism. It has been shown in previous works

that during extended recovery which is also known as continuous recrystallization (cRX) the deformation microstructure is converted into a grain structure merely through extended recovery reactions retaining the local texture [19 24]. Fig. 4d shows the grain size distributions of the heat treated samples in which there is no appreciable change between them (Fig. 4d, calculated taking into account only high angle grain boundaries HAGB).

To further analyze features of recovery, the deformed fraction of the microstructures for the heat treated samples are presented in Fig. 5a, b and c. It can be seen that at 250 and 300 °C several grains show regular arrays of LAGB which is typical of a recovery process, and the related grain orientations in these two cases show a markedly angular distribution towards TD (Figs. 5a and b, respectively). In contrast, the sample annealed at 350 °C has fewer deformed grains than in the two previous cases and their related orientation do not show a markedly distribution towards TD anymore (Fig. 5c). With the purpose to show the development of deformed and recrystallized grains with basal and non-basal orientation the following assumption was used. In this analysis presented in Fig. 5d, any grain with its c-axis nearly parallel (maximum deviation of 20 °) to the normal direction of the sheet is considered as basal, whereas grains with higher deviation are accounted in the non-basal fraction. This tolerance was arbitrarily chosen, but a variation of this parameter qualitatively does not change the results. From the EBSD maps, it is possible to separate grains with a certain crystal orientation direction and relate them with a reference frame that in this case is the ideal rolling coordinates. This analysis allows us to distinguish the effect of grains with their basal planes that are almost parallel to the sheet plane. It can be seen that the area fraction of deformed non-basal grains decreases monotonically with increasing the annealing temperature, while the fraction of deformed basal grains remains almost constant. Contrarily, in the recrystallized fraction of the microstructure, the area fraction of recrystallized non-basal grains is rather comparable in the three cases, whereas the area fraction on basal grains shows a monotonic increase with increasing the annealing temperature. The present result suggests that there is a preferential growth of recrystallized grains with basal orientation at expense of deformed grains with non-basal orientation. This effect could be a sign of a dRX process, in which the growth of strain-free basal grains is driven by the stored energy of non-basal grains rather than at expense of deformed basal grains. This is evident because a similar fraction of deformed basal grains prevail at all annealing temperatures.

On the other hand, the development of recrystallized non-basal grains is slightly affected with increasing the annealing temperature. As shown in Fig. 4, several grains with non-basal

orientations are conglomerated in sections that can be related to earlier elongated grains e.g grains deformed by prismatic <a> slip. A close inspection in the recrystallized fraction of the microstructure of samples annealed at 250 and 350 °C (Fig. 7a and b, respectively) shows that some recrystallized non-basal grains (marked with arrows) are located near grains having features of recovery as shown in Fig. 5a and c. More importantly, the deformed and recrystallized grains in the vicinity of such zones have similar orientations. It is therefore, reasonable to assume that the origin of some recrystallized non-basal grains is a result of the activation of cRX.

It is worth to highlight that features of recovery and cRX are present in grains that were most likely deformed by prismatic <a> slip, whereas the grains likely deformed by pyramidal <c+a> slip have been replaced by equiaxed recrystallized grains.

This fact indicates that the involved deformation mode is playing an important on the recrystallization behaviour. For instance, in single crystals deformed in single glide, recovery on annealing occurs, because the dislocation structure does not contain the heterogeneities and orientation gradients needed to provide a nucleation site [24]. Indeed, this phenomenon has been observed in Zinc crystals which recover without recrystallization during a heat treatment even though they were subjected to an extensive plastic strain [25].

The above observation resembles what happens during DRX in Mg alloys. In this regard Kaibyshev et al. [26] reported that DRX is a rapid process when slip of <a> dislocations takes place on basal, prismatic and pyramidal planes. When only two slip systems control the deformation such as basal and prismatic slip of <a> dislocations the DRX is slowed down. This is because, <c+a> dislocations are required for the formation of 3D recrystallization nuclei, which can therefore trigger more effectively the recrystallization process [27].

In addition to the above considerations, another important factor that can influence the rate of recrystallization is the amount of strain contained in each type of deformed grain. Farzadfar et al.[28] have shown that in hot rolled Mg-2.9Y and Mg-2.9Zn (wt%) alloys, elongated grains with orientation close to (0001) contain dense and fine sub-grain structures and can store up to 20 times more energy than elongated grains with orientation close to $(2\bar{1}\bar{1}0)$ which consequently have coarse sub-grain structures. The dense and fine substructures in grains with orientation close to (0001) lead to a higher degrees of recrystallization with finer grains than the coarse substructure found in grains with orientation close to $(2\bar{1}\bar{1}0)$.

Ex-situ EBSD analysis was performed before and after a short recrystallization annealing in order to identify the origin of the recrystallization sites and relate them with a respective recrystallization mechanism. Fig. 6 shows the microstructural development of a sample

measured in as-rolled condition and after two consecutive heat treatments at 250 °C for 3 and 15 min (Figs. 6a, d and g, respectively). The IPF map presented in Fig. 6a of the as-rolled condition shows comparable characteristics to the one shown in Fig. 2a. There is a combination of large elongated grains with the aforementioned orientations. Once again the separation of the fraction of the microstructure with a low internal misorientation of GOS<0.5° is shown in Fig. 6b. The validation of the recrystallized fraction of grains given by the GOS analysis is conducted. This is necessary because in some grains the amount of stored strain can be underestimated or overestimated, especially if the GOS is normalized by the grain size diameter [29]. Consequently, in addition to the GOS analysis, in fig. 6c an IQ map is depicted with superimposed KAM map as an additional indicator of zones with high stored strain i.e. a combination of the IQ and the misorientation base approach. The KAM maps are calculated based on the degree of misorientation between a kernel (measuring point) and its neighbours [30]. That in the case of this study, the KAM is calculated using the third neighbour. The zones (grains) with low strain in IQ-KAM maps presented in Fig. 6c are in good agreement with the grains considered as recrystallized by the GOS analysis. After the short heat treatments, the microstructure exhibits noticeable changes in the microstructure. On one hand, it is seen in Fig. 6e and 6h that grains start to develop and grow faster in shear bands zones, as well as inside elongated grains with orientations close to (0001). As indicated by the open arrows, it is possible to locate the recrystallization nuclei. They recrystallization nuclei are in zones where $\{10\bar{1}1\}$-$\{10\bar{1}2\}$ double twins was activated as shown in the squares with the dashed white line (the double twin boundary coloured in green is shown in an amplified IQ map inserted in Fig. 6a). This gives good experimental evidence that the preferred mechanism is dRX in large elongated grains with orientations close to (0001). On the other hand, the $\{10\bar{1}2\}<10\bar{1}\bar{1}>$ tension twins which present in the large grain with orientation close to $(2\bar{1}\bar{1}0)$ are stable. It was possible to find good evidence that the activation of cRX is preferred grains with this orientation. As indicated by the full arrows there are zones that show features of extended recovery in which there is the formation of LAGB and the growth of the recovered zone. The growth of the recovered zone and the formation of LAGB and HAGB are clearly seen in the amplified insets presented in Figs. 6a, d and g.

In this study, the present results correlate well with the fact that within grains deformed preferentially by prismatic <a> slip the recrystallization mechanism was cRX whereas in the grains deformed by pyramidal <c+a> slip was dRX. Both recrystallization mechanisms and recovery lead to the formation of recrystallized grains with the concurrent reduction of the

stored strain as shown in Fig. 6f and 6i. It should be mentioned that cRX seems to be a slower mechanism than dRX and that the recovered areas could promote the growth of grains with their c-axis close to (0001) orientation. The activation of this cRX has most likely also been hindered since higher annealing temperatures are commonly used in which dRX and grain growth dominates the texture formation.

During annealing of conventionally rolled AZ31 sheets, it is widely accepted that features from the rolling texture such as tilted basal planes (e.g. a double peak in the basal pole along RD) are replaced by a single peak as a result of grain growth which leads to the formation of the basal type texture [16]. Yet, as shown in this work it can be possible to retain interesting features from the rolling texture by increasing the relative activity of cRX during annealing at lower temperatures and by retaining recovered grains with off-basal orientation.

Still, Huang et al. [31] demonstrated the potential of activating dRX during annealing of hot rolled AZ31 sheets. In their work, it was reported that the increase activity of pyramidal <c+a> slip might be the reason for the weakening of the basal texture intensity if the rolling trials are carried out at very high rolling temperatures i.e. 525 °C. Additionally, they observed that such an increase in the activity of pyramidal <c+a> slip would also be responsible for a further texture weakening during annealing. This is because new grains were formed with a largely tilted c-axis in which dRX was supposed to be the dominant recrystallization mechanism [32].

As addressed above, it is likely that cRX and dRX are activated at all the annealing temperatures used in this work and that they can trigger the formation of grains with specific orientations. However, it is known that the development of an annealing texture does not cease when primary recrystallization is complete. Changes in texture continue during further grain growth and the final texture is not necessarily representative of the texture present when primary recrystallization is complete [24].

Consequently, in an attempt to separate the recrystallization with grain growth effects, the recrystallized fraction of the microstructure was separated according to its average recrystallized grain size (RGS). Accordingly, the textures of recrystallized fraction of the microstructures with grain size smaller and coarser than the RGS are presented in Fig. 7c. The RGS for the samples heat treated at 250, 300 and 350 °C are 9.5, 9.7 and 9.8 μm respectively (the width of the grain size distribution is between 3.1 and 3.6 μm). At 250 and 300 °C the textures are very comparable, the small recrystallized grains are characterised by the basal type texture whereas the coarser grains present comparable features with the deformation texture for each condition. It can also be observed that as the annealing temperature increases,

the texture intensity of the small recrystallized grains increases keeping the basal texture. This behaviour gives a hint that oriented growth is active for the new recrystallized grains having the basal texture. However, it is difficult to separate the pure effect that have recrystallized basal grains growing at expense of stored strain of the neighbouring grains (i.e. growth of grains during primary recrystallization) from the effect that have grains growing in order to decrease the grain boundary area and thus reducing the internal stored energy. Table 1 shows a separation of recrystallized grains (GOS<0.5°) according to the crystal orientation and grain size. A slight increase of the grain size of the basal fraction (tilt angle <20°) is found with increasing temperature, whereas the non-basal grains show the opposite, specifically if the result at 300 and 350 °C are compared.

Table 1. Average recrystallized grain size (GOS<0.5°) at different heat treatments for grains having basal (deviation of the c-axis with respect to ND <20°) and non-basal orientations (deviation >20°), the variation of the width of the grain size distribution is in between 3.3 and 3.8 µm.

Heat treatment temperature for 30 min	*250 °C*	*300 °C*	*350 °C*
Grain size: Basal [µm]	8.7	9.4	9.8
Grain size: Non basal[µm]	9.7	9.8	8.6

Another important aspect to stress from Fig. 7c is that the coarse recrystallized grains present at 250 and 300 °C keep the $\{0001\}\langle 10\bar{1}0\rangle$ texture component without increase of the texture intensity. Evidence of degradation of the $\{0001\}\langle 10\bar{1}0\rangle$ texture component during grain growth in Ti alloys has been reported by Bunge et al. [33]. Therefore, the origin of the coarse recrystallised grains in this study can be assumed as a result of cRX since there is no degradation of the $\{0001\}\langle 10\bar{1}0\rangle$ texture component and, therefore, it can also be assumed that grain growth is not playing a significant role at 250 and 300 °C. In the case of the sample annealed at 350 °C, the fraction of coarse grains show degradation of the $\{0001\}\langle 10\bar{1}0\rangle$ texture component. Furthermore, the basal texture of those coarse recrystallized grains shows a noticeable sharpening of the texture intensity which can be attributed to grain growth.

It is noteworthy that although the coarse recrystallized non-basal grains would have the possibility to grow at expense of smaller grains, they are very stable at all temperatures. This might be a significant difference in the grow behaviour of non-basal grains in Mg-Al-Zn

alloys compared to Mg-RE added alloys. It has been reported recently that in a Mg-Gd alloy, non-basal grains do have a growth advantage over basal grains due to their size which leads to the strengthening of other orientations to the basal one [34].

Further investigation is necessary to analyse the characteristics of grain boundaries i.e. grain boundary energy per unit surface and grain boundary mobility in the basal and non-basal grains in order to understand the relationship between texture and preferential grain growth.

4. Conclusions

In summary, the microstructure and texture development during isochronal annealing of a TRC-AZ31 alloy was analysed in terms of deformation and recrystallization mechanisms. It was found that the appearance of elongated grains and $\{10\bar{1}1\}$-$\{10\bar{1}2\}$ double twins in the as-rolled microstructure leads to a distinct in rolling texture to the basal type texture. The main deformation modes for the formation of elongated grains are pyramidal <c+a> and prismatic <a> slip.

Recovery, cRX and dRX, and growth of grains were the main mechanisms involved in the microstructural development during the isochronal annealing treatments used in this work.

The activity of pyramidal <c+a> slip was linked with and enhanced recrystallization process in which dRX was the dominant recrystallization mechanism. Zones within $\{10\bar{1}1\}$-$\{10\bar{1}2\}$ double twins serve as the recrystallization nuclei for the formation of new strain free grains. The preferential growth of recrystallized basal grains was driven by stored energy contain in deformed grains with non-basal orientation. This is related with the growth of recrystallized grains during primary recrystallization.

Recovery and cRX occurred preferentially in elongated grains deformed by prismatic <a> slip. The activation of cRX plays an important role on microstructural development 300 and 250 °C. During annealing at these temperatures, the deformed microstructure is replaced by new recrystallized grains and recovered grains. Consequently, it is possible to observe features of the rolling texture.

The growth of grains with orientations close to (0001) dominates the texture development at 350 °C leading to the formation of the well-known basal type texture.

Acknowledgments

The financial support of the Deutsche Forschungsgemeinschaft (DFG), Grant no. (LE1395/6-1) is gratefully acknowledged. The assistance of Petra Fisher at HZG with the EBSD measurements is appreciated.

References

[1] K. Hantzsche, J. Bohlen, J. Wendt, K.U. Kainer, S.B. Yi, D. Letzig. Scripta Mater 63 (2010) 725-730

[2] D. Wu, R.S. Chen, E.H. Han, J Alloy Comp 509 (2011) 2856-2863].

[3] T. Al-Samman, X. Li. Mater Sci Eng A528 (2011) 3809-3822

[4] J. Bohlen, M.R. Nürnberg MR, J.W. Senn, D. Letzig, S.R. Agnew. Acta Mater 55 (2007) 2101-2112

[5] I. Basu, T. Al-Samman. Acta Mater 67 (2014) 116-133

[6] E.A. Ball, P.B. Prangnell, Scripta Mater 31 (1994) 111-116

[7] T. Al-Samman, Mater. Sci. Eng, A560 (2013) 561-566

[8] N. Stanford, M.R. Barnett, Mater Sci Eng A496 (2008) 399-408

[9] J.P. Hadorn, K. Hantzsche, S. Yi, J. Bohlen, D. Letzig, S.R. Agnew, Metall Mater Trans A43 (2012) 1363-1375

[10] J. Victoria-Hernandez, S. Yi, D. Letzig, D. Hernandez-Silva, J. Bohlen, Acta Mater 61 (2013) 2179-2193

[11] J. Victoria-Hernandez, D. Hernandez-Silva, S.B. Yi, D. Letzig, J. Bohlen, Mater. Sci. Eng. A 503 (2011) 411-417

[12] R. Hielscher, H. Schaeben. J Appl Crystallgr 41 (2008) 1024-1037

[13] G. Kurz, J. Bohlen, D. Letzig, K.U. Kainer, Mater. Sci. Forum 765 (2013) 205-209

[14] S.R. Agnew, M.H. Yoo, C.N. Tomé, Acta Mater. 49 (2001) 4277-4289

[15] X. Huang, K. Suzuki, Y. Chino, Mater. Sci. Eng. A 560 (2013) 232-240

[16] L.W.F. Mackenzie, M. Pekguleryuz, Mater. Sci. Eng. A 480 (2008) 189-197

[17] S. Yi, J. Bohlen, F. Heinemann, D. Letzig, Acta Mater. 58 (2010) 592-605

[18] Partridge PG. Metall Rev 12 (1967) 169-194

[19] K.Y. Zhu, D. Chaubet, B. Bacroix, F. Brisset, Acta Mater. 53 (2005) 5131-5140

[20] F. Wagner, N. Bozzolo, O. Van Landuyt, T. Grosdidier, Acta Mater. 50 (2002) 1245-1259

[21] S.L. Couling, J.F. Pashak, L. Sturkey, Trans. ASM 54 (1959) 94-107

[22] S. Dziaszyk, E.J. Payton, F. Friedel, V. Marx, G. Eggeler. Mater Sci Eng A 527 (2010) 7854-7864

[23] S. Yi, H.Z. Brokmeier, D. Letzig, J alloys and Comp. 506 (2010) 364-371

[24] Humphreys FJ, Hatherly M. Recrystallization and related annealing phenomena. Oxford: Elsevier; 2004. p. 211, 380

[25] O. Haasen, E. Schmid, J. Phys. 33 (1925) 413

[26] R. Kaibyshev, B. Sokolov, A. Galiyev. Texture Microstructure 32 (1999) 47-63

[27] A. Galiyev, R. Kaibyshev, G. Gottstein. Acta Mater 49 (2001) 1199-1207

[28] S.A. Farzadfar, E. Martin, M. Sanjari, E. Essadiqi, M.A. Wells, S. Yue. Mater Sci Eng A 534 (2012) 209-219

[29] N. Allain-Bonasso, F. Wagner, S. Berbenni, D. Field. Mater. Sci. Eng. A 548 (2012), 56-63

[30] S. I. Wright, M.M. Nowell, D.P. Field. Microsc. Microanal. 17 (2011), 316-329

[31] X. Huang,K. Suzuki, Y. Chino, M. Mabichi, J. alloys and Comp. 537 (2012) 80-86

[32] X. Huang, K. Suzuki, Y. Chino. J. Alloys and Comp. 509 (2011) 4854-4860

[33] H.J. Bunge, C.U. Nauer-Gerhardt, Titanium Science and Technology, vol. 3, DGM, (1985) 173-177

[34] W.X. Wu, L. Jin, Z.Y. Zhang, W.J. Ding, J. Dong. J. Alloys Comp. 585 (2014) 111-119

Tables:

Table 1. Average recrystallized grain size (GOS<0.5°) at different heat treatments for grains having basal (deviation of the c-axis with respect to ND <20°) and non-basal orientations (deviation >20°), the variation of the width of the grain size distribution is in between 3.3 and 3.8 µm.

Heat treatment temperature for 30 min	*250 °C*	*300 °C*	*350 °C*
Grain size: Basal [µm]	8.7	9.4	9.8
Grain size: Non basal[µm]	9.7	9.8	8.6

Figure captions:

Fig. 1 Optical microstructures of the (a) as-cast condition of the twin roll cast strip and (b) after hot rolling at 450 °C using hot rollers at 230 °C. (c) and (d) global texture measurements presented in terms of the (0001) and $(10\bar{1}0)$ pole figures for the as-cast and AR conditions.

Fig. 2 OM in AR condition (a), pattern quality map showing orientation of selected grains (b), OM for deformed (GOS>0.5°) and recrystallized (GOS<0.5°) fraction of the microstructure (c) and (d) respectively. Textures presented in terms of the (0001) and $(10\bar{1}0)$ pole figures calculated using the EBSD data.

Fig. 3 Optical microstructures of heat treated samples at (a) 250 °C, (b) 300 °C and (c) 350 °C for 30 min. (d), (e) and (f) global texture measurements presented in terms of the (0001) and $(10\bar{1}0)$ pole figures for the heat treatments at 250 °C, 300 °C and 350 °C respectively.

Fig. 4 OM of microstructures after annealing 30 min at 250 °C (a), 300 °C (b) and 350 °C (c), grain size distribution at all conditions (d) (HAGB and LAGB coloured in black and grey respectively).

Fig. 5 Fraction of deformed microstructure (GOS>0.5°) with related orientations for samples annealed at 250 °C (a), 300 °C (b) and 350 °C (c), and fraction of deformed and recrystallized grains with basal and non-basal orientation (d). HAGBs ($\theta > 15^\circ$) are coloured in blue, LAGBs ($2^\circ < \theta < 15^\circ$) are coloured in green, dashed lines are presented to guide the eyes.

Fig. 6 OM of the microstructure in (a) AR condition, (d) after being annealed at 250 °C for 3 min and (g) after being annealed at 250 °C for 15 min. Recrystallized fraction of the microstructure using GOS<0.5° in (b) AR condition, (e) after being annealed at 250 °C for 3 min and (h) after being annealed at 250 °C for 15 min. (c) IQ map with a superimposed KAM map for the (c) AR condition and (f) after 3 min at 250 °C and (i) after annealing at 250°C for 15 min.

Fig. 7 OM of recrystallized fraction of the microstructure (GOS<0.5°) annealed at 250 °C (a) and 350 °C (b), and (c) fractions of the microstructure of recrystallized grains smaller and coarser than RGS at 250, 300 and 350 °C respectively.

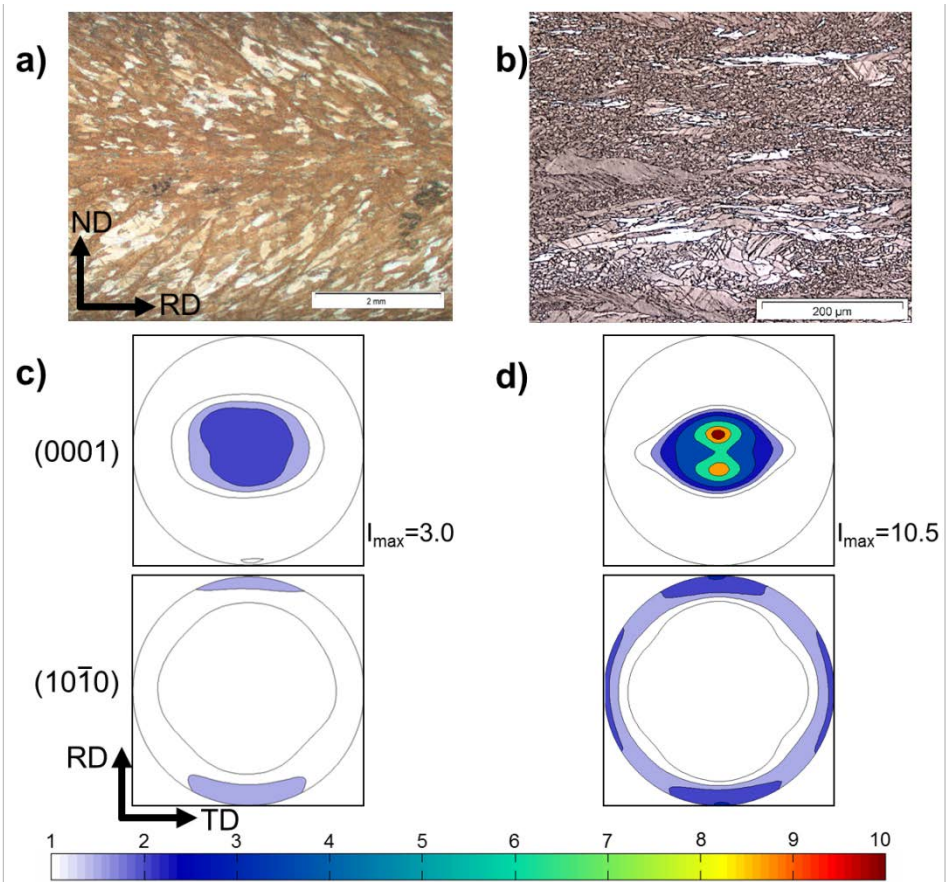
a)
ND
RD
2 mm
b)
200 µm
c)
(0001)
I_{max}=3.0
d)
I_{max}=10.5
(10$\bar{1}$0)
RD
TD
1 2 3 4 5 6 7 8 9 10

Fig. 1

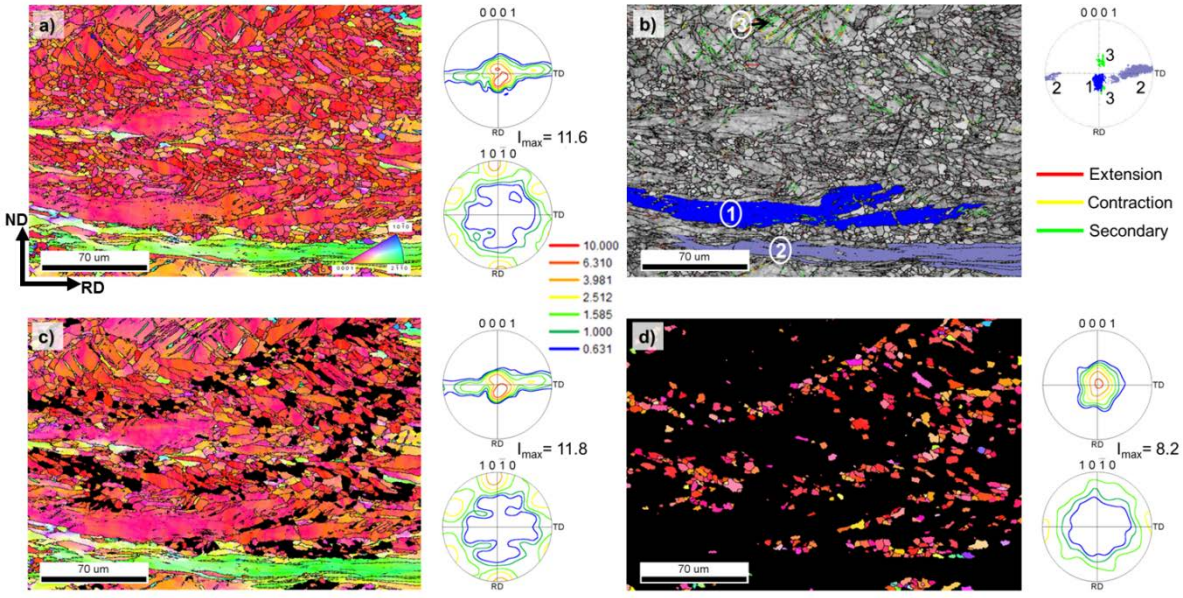
a)
ND
RD
70 um
0 0 0 1
TD
RD
I_{max}= 11.6
1 0 1 0
10.000
6.310
3.981
2.512
1.585
1.000
0.631
b)
70 um
Extension
Contraction
Secondary
c)
70 um
I_{max}= 11.8
d)
70 um
I_{max}= 8.2

Fig. 2

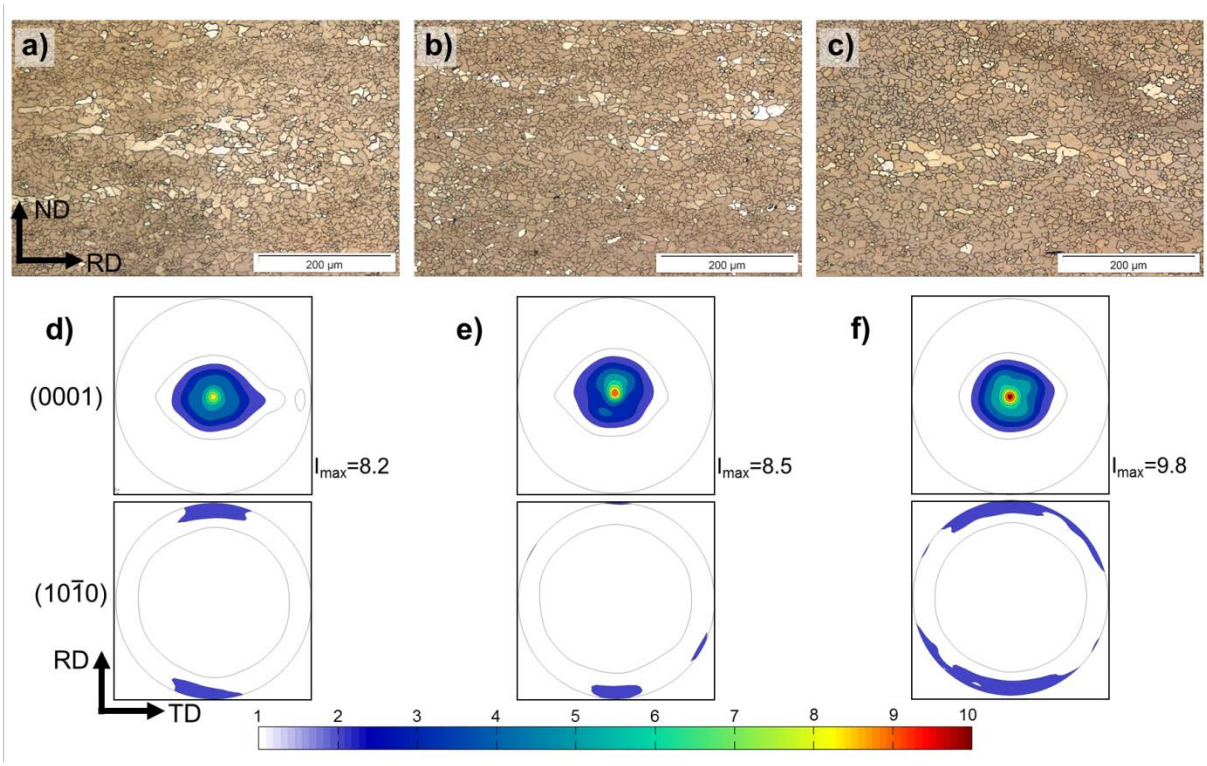
a)
b)
c)
ND
RD
200 µm
d)
e)
f)
(0001)
(10$\bar{1}$0)
I_{max}=8.2
I_{max}=8.5
I_{max}=9.8
RD
TD
1 2 3 4 5 6 7 8 9 10

Fig.3

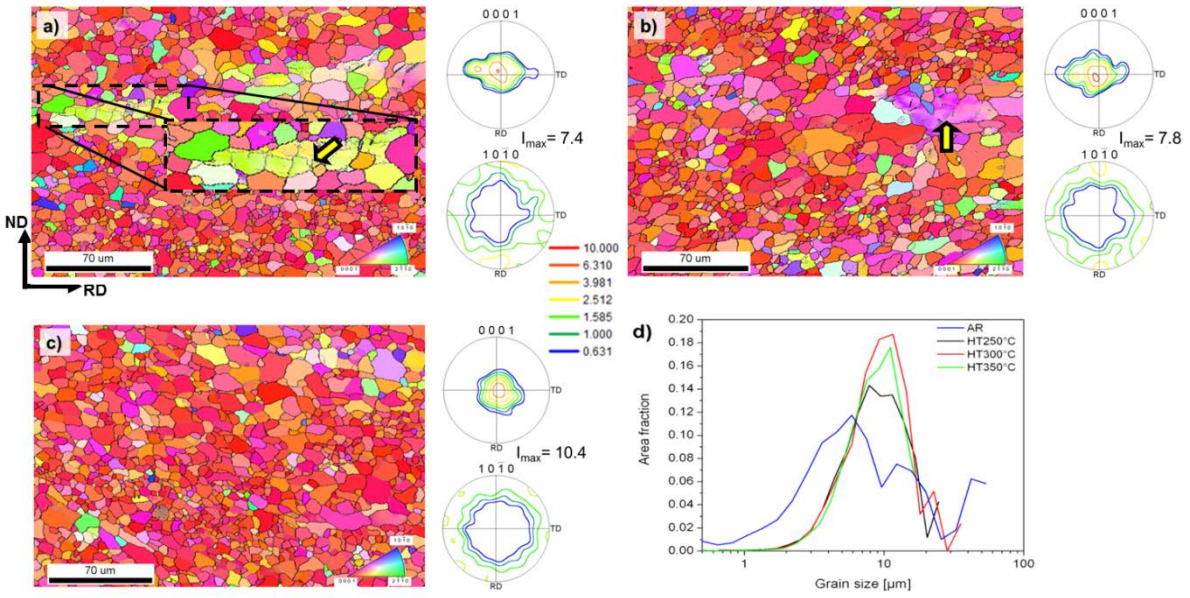
a)
b)
c)
d)
ND
RD
70 um
0 0 0 1
1 0 1 0
TD
RD
I_{max}= 7.4
I_{max}= 7.8
I_{max}= 10.4
10.000
6.310
3.981
2.512
1.585
1.000
0.631
AR
HT250°C
HT300°C
HT350°C
Area fraction
Grain size [µm]

Fig.4

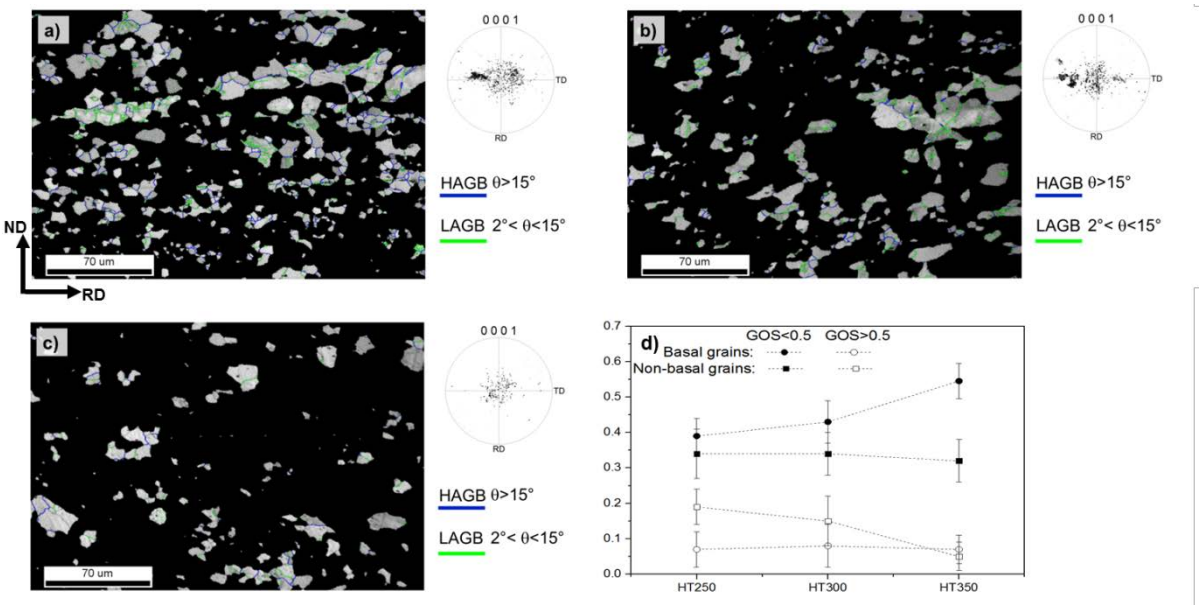
a)
b)
c)
d)
0001
TD
RD
HAGB θ>15°
LAGB 2°< θ<15°
70 um
ND
RD
GOS<0.5 GOS>0.5
Basal grains:
Non-basal grains:
0.7
0.6
0.5
0.4
0.3
0.2
0.1
0.0
HT250
HT300
HT350

Fig. 5

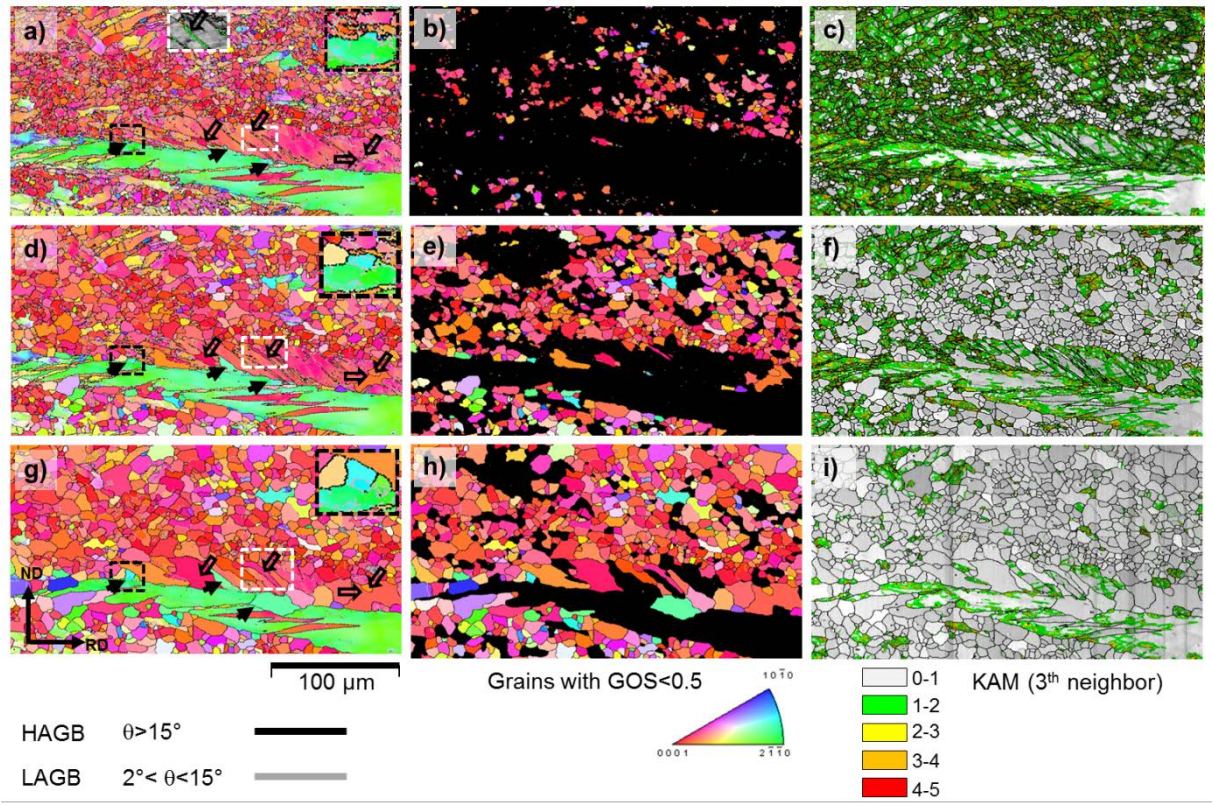
a)
b)
c)
d)
e)
f)
g)
h)
i)
ND
RD
100 μm
Grains with GOS<0.5
0001
$10\bar{1}0$
$2\bar{1}\bar{1}0$
HAGB θ>15°
LAGB 2°< θ<15°
0-1
1-2
2-3
3-4
4-5
KAM (3th neighbor)

Fig. 6

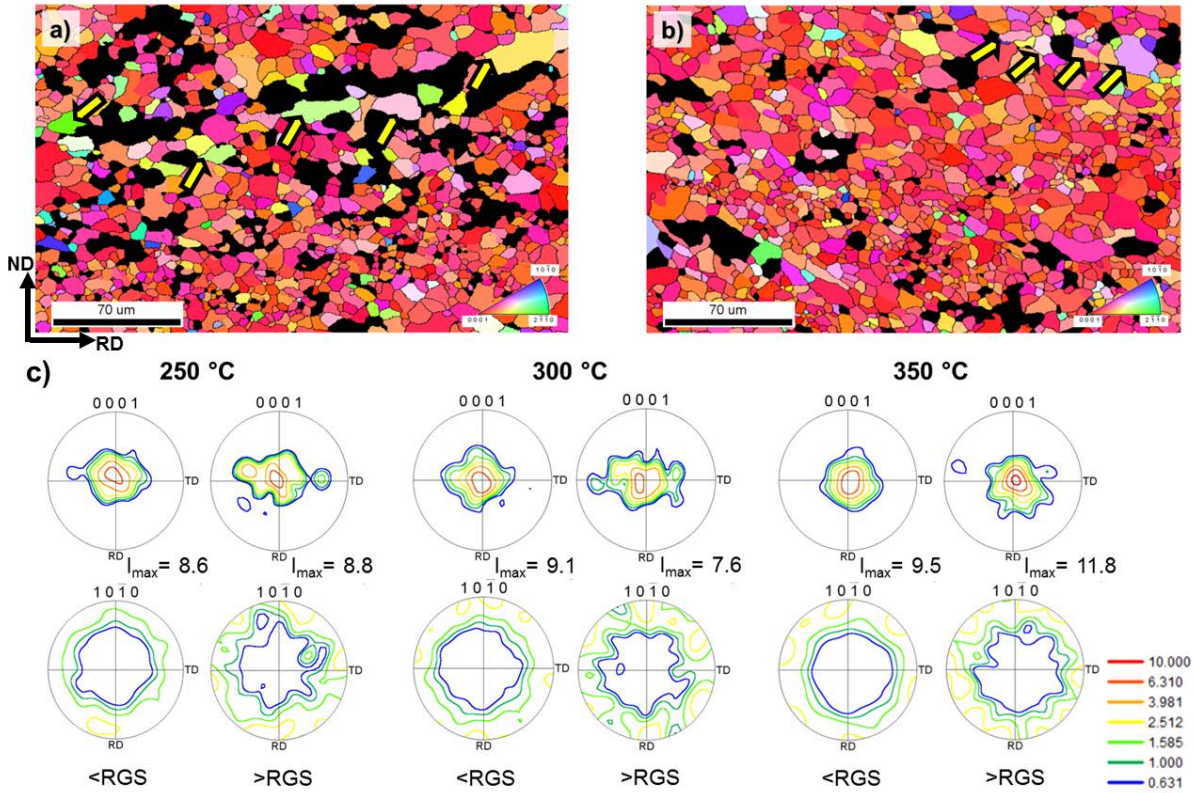
a)
b)
ND
RD
70 um
70 um
c)
250 °C
300 °C
350 °C
0001
1010
TD
RD
I_{max}= 8.6
I_{max}= 8.8
I_{max}= 9.1
I_{max}= 7.6
I_{max}= 9.5
I_{max}= 11.8
<RGS
>RGS
10.000
6.310
3.981
2.512
1.585
1.000
0.631

Fig.7